IOP Publishing Physica Scripta
Phys. Scr. 95 (2020) 045206 (12pp) https://doi.org/10.1088/1402-4896/ab3c3f

On the onset of entropy generation for a nanofluid with thermal radiation and gyrotactic microorganisms through 3D flows

M Sohail[1,4], R Naz[1] and Sara I Abdelsalam[2,3,4]

[1] Department of Applied Mathematics and Statistics, Institute of Space Technology, PO Box 2750, Islamabad 44000, Pakistan
[2] Basic Science, Faculty of Engineering, The British University in Egypt, Al-Shorouk City, Cairo 11837, Egypt
[3] Instituto de Matemáticas - Juriquilla, Universidad Nacional Autónoma de México, Blvd. Juriquilla 3001, Querétaro, 76230, México

E-mail: muhammad_sohail111@yahoo.com, sara.abdelsalam@bue.edu.eg, siabdelsalam@yahoo.com and siabdelsalam@im.unam.mx

Received 18 April 2019, revised 9 June 2019
Accepted for publication 15 July 2019
Published 11 February 2020

Abstract

This work presents the entropy analysis of Maxwell nanofluid containing gyrotactic microorganism in the presence of homogeneous–heterogeneous reactions with modified heat and mass flux models. Modified models are presented by utilizing Cattaneo–Christov heat flux and generalized Fick's law. Derived equations which shows the considered flow situation are modeled in the form of PDEs under boundary layer theory, then suitable transformation is applied to convert arising PDEs into a set of transformed ODEs which are then solved using a powerful scheme namely optimal homotopy analysis procedure. Special cases of some published work are found to be in excellent agreement of our work. The impact of physical parameters on velocity, temperature, concentration, reaction rate, concentration of motile microorganism, and entropy generation are discussed graphically. Finally, the convergence of applied scheme is presented in tabular form which confirms the efficiency of applied method. It is reported that entropy generation increases for higher values of radiation parameter and Brinkman number, whereas Bejan number is reduced for the higher values of radiation and magnetic parameters. Also, fluid temperature and concentration fields are reduced by augmenting the values of Prandtl and Schmidt numbers.

Keywords: Maxwell fluid, gyrotactic microorganism, homogeneous–heterogeneous reactions, heat generation, thermal radiation, thermal conductivity

(Some figures may appear in colour only in the online journal)

Nomenclature

$\mathbf{B}$	magnetic field
B_0	strength of magnetic field
$u_1^*,\ v_1^*,\ w_1^*$	velocity components
δ_0	fluid moderation time
ν_1	kinematic viscosity
ρ_f	fluid density
ρ_l	microorganisms density
ρ_p	nanoparticles density
g_a	gravitational acceleration
β_a	volume expansion coefficient
χ_a	ratio of operational heat capability of the nanoparticle to that of fluid
a_1	Brownian diffusion coefficient
a_2	thermophoresis diffusion coefficient
Q_a	heat generation/absorption parameter

[4] Authors to whom any correspondence should be addressed.

l	microorganism concentration
α_c^*	rate constant
ξ	dimensionless variable
(ε_2)	concentration difference parameter
D_1	non-dimensional fluid relaxation time
Sc	Schmidt number
χ_H	heat source/sink parameter
χ_B	Brownian motion parameter
$\lambda_1,\ \lambda_2$	non-dimensional relaxation time parameters for temperature and concentration
P_1	Peclet number
N_s	strength of heterogeneous reactions
ε_3	diffusion parameter
c_p	specific heat
$f'(\xi),\ g'(\xi)$	dimensionless velocities
$\varphi(\xi)$	dimensionless concentration
$\widetilde{\mathbf{Q}}$	heat flux
T	fluid temperature
C	fluid concentration
$\widetilde{\mathbf{Q}}_r$	radiative heat flux
$\widetilde{\mathbf{J}}$	mass flux
T_∞	ambiant fluid temperature
C_∞	ambiant fluid concentration
ρ_∞	ambiant fluid density
$A_1^*,\ B_1^*$	concentrations of chemical species corresponding to A and B
ξ_c	chemotaxis parameter
D_c	microorganism diffusion coefficient
$\delta_1,\ \delta_2$	diffusion constants
ε_E	thermal relaxation time
ε_C	concentration relaxation time
K_a	thermal conductivity
D_a	molecular diffusivity
M	magnetic parameter
ε_1	temperature difference parameter
Pr	Prandtl number
β_1	ratio parameter
χ_T	thermophoresis parameter
χ_R	thermal radiation parameter
k_1	strength of homogeneous reactions
L_1	bio convection Lewis number
Sr	Schmidt number for homogeneous–heterogeneous reactions
Br	Brinkman number
$E_G(\xi)$	entropy generation
$B_E(\xi)$	Bejan number
$\theta(\xi)$	dimensionless temperature

1. Introduction

Flow past over a stretched surface has numerous applications in various discipline of applied sciences. In 1867, Maxwell noticed that some fluids like air obeys the characteristics of viscous and elastic behaviors mentioned in [1–3] and references therein. Many fluids such as glycerin, crude oils or some polymeric solutions behave as Maxwell fluids [4–6]. Vieru *et al* [7] studied fractional Maxwell fluid flow over a plate. They computed the exact solutions for velocity by operating Fourier and Laplace transforms. Fetecau *et al* [8] explored the relaxation effects of unsteady boundary layer flow of Maxwell fluid which cannot be foreseeable in other types of non-Newtonian fluids over a stretching sheet. Exact solutions of Stokes second problem for Maxwell fluid have been computed via Laplace transform. They proved that for large times their computed solutions ease to the steady-state solutions which are periodic and independent of the given initial data. Variable thermo-physical characteristics of upper convicted Maxwell fluid over a melting surface is reported by Adegbie *et al* [9]. Similarity solutions of liquid flow over a melt surface where the flow is the result of thermal and dissolved stratification have been theoretically reported by them. Bearing of thermal stratification, variable viscosity with temperature dependent thermal conductivity is deliberated. Derived set of equations are solved numerically via Runge–Kutta procedure along with shooting scheme. Results in the form of graphs and tables for the dimensionless stress, heat transfer, mass transfer, concentration, and velocity and temperature fields are presented and described for various values of the emerging parameters. Applications in the fields of transportation, and chemical and metallurgical sectors are prominent due to heat enhancement that is encountered due to the existence of microorganisms with magnetic field. Numerical solutions of stagnation point flow of Maxwell nanofluid with heat transfer past a stretched surface is scrutinized by Nadeem *et al* [10]. In their investigation they considered that the fluid impinges on the wall obliquely and their considered model incorporates the effects of Brownian motion and thermophoresis. They converted the governing partial differential equations into nonlinear ordinary differential equations by utilizing similarity transformation. The resulting ordinary differential equations are tackled analytically by homotopy analysis method. Numeric values of different amounts of interest are calculated and described by tables and also have indicated that a boundary layer is formed when the elongated speed of the surface is smaller than the non-viscid free flow rate. Soret and suction effects of Maxwell saturated Ferrofluid flow are investigated by Majeed *et al* [11] with chemical reaction and heat transfer phenomena past a permeable stretching surface under the influence of magnetic dipole. The

sheet was assumed to be permeable in a semi-infinite domain. Solutions of the transformed nonlinear differential equations is calculated by Runge–Kutta technique along with shooting routine with MATLAB. The ferromagnetic flow past a stretched surface with heat, mass, Brownian movements and thermophoresis possessions in the incidence of magnetic dipole are addressed by Hayat *et al* [12]. The obtained nonlinear expressions have been computed numerically by means of shooting scheme. Graphical results for the impact of different variables are shown and analyzed. Temperature and concentration gradients are numerically computed with the help of tables. Their results described that ferromagnetic variable escalates the thermal field. Ramzan *et al* [13] studied the mixed convective flow of Maxwell nanofluid through porous medium with Soret and Dufour effects and appearing equations are handled analytically. Transformed nonlinear equations are solved optimally with the help of Mathematica package BVPh 2.0. Graphs are plotted for numerous emerging parameters for velocity, temperature and concentration disseminations solutions and discoursed accordingly. For more recent contributions in nanofluid and magnetic field effects, reader is referred to [14–19] and to the references therein.

Chemical responding systems are categorized by homogenous and heterogeneous reactions that respond contrarily in the incidence or nonexistence of a chemical agent. Belongings of chemical reactions is specifically momentous in food handling, manufacturing of tiles, polymer fabrication, metallurgy and hydrometallurgical industry, chemical processing apparatus design and crops destruction via freezing etc. Heterogeneous–homogeneous reactions in flow of viscous fluid are examined by Merkin [20]. Homogeneous reaction for cubic auto catalyst and heterogeneous reaction on catalyst surface is examined in his experiment. Numerical solutions of the arising expressions disclose that the homogeneous reaction is dominant in a narrow region situated away from the surface and also an asymptotic analysis is achieved. Chaudhary *et al* [21] scrutinized heterogeneous–homogeneous reactions with equal diffusivities for the flow of viscous fluid having isotherm. They computed the solutions for homogeneous–heterogeneous reactions when diffusion coefficients of the reactant and auto catalyst are not same. Stagnation point flow with heterogeneous–homogeneous reactions by stretched surface is scrutinized by Bachok *et al* [22]. They computed the solutions of subsequent equations numerically via Keller-box procedure. Viscous fluid flow having nanomaterial with heterogeneous–homogeneous reactions produced by a penetrable elongating surface is addressed by Kameswaran *et al* [23]. They scrutinized the impression of copper-water and silver-water nanofluids in their deliberation. Analytic solution for unsteady hydro magnetic flow through a stretched surface with heterogeneous–homogeneous reactions are offered by Imtiaz *et al* [24]. They reported that the surface drag force upsurges by wavering curvature parameter and surface concentration shrinkages for homogeneous reaction parameter and unsteadiness parameter. Flow of carbon nanotubes with heterogeneous–homogeneous reactions over a nonlinear stretched surface with variable thickness are conveyed by Hayat *et al* [25]. Convergence control parameters for series solutions and residual errors for water, kerosene and engine oils in the occurrence of single wall (SWNTs) and multi wall (MWNTs) carbon nanotubes are discoursed via optimal homotopy analysis method (OHAM). Some other endeavors on heterogeneous–homogeneous reactions can be accessed through the inspections mentioned in [26, 27].

The mechanism of bioconvection is established due to the upswing of the suspensions of motile microorganisms. The phenomenon of bio convection was first observed by Kuzenstov [28]. The collaboration of Geng and Kuzenstov [29–31] considers the mixture of nanoparticles and microorganisms. They reported that due to the inclusion of gyrotactic microorganisms, stability of the nanoparticles increases. Involvement of time dependent second grade fluid containing nanoparticles and gyrotactic microorganisms between two parallel plates are studied by Zuhra *et al* [32]. They reported that fluid velocity accelerates for increasing values of unsteadiness parameter and it shrinkages for the augmenting values of viscoelastic parameter. Rehman *et al* [33] studied the viscous nanofluid flow containing gyrotactic microorganisms over a vertical stretching sheet. After the utilization of similarity transformation, governing fluid flow equations are reduces to the function of single independent variable and then solution is computed via shooting scheme. They analyzed that the density of motile microorganisms decreases by augmenting the values of bio convection Schmidt and Peclet numbers. For the interest of readers, some other studies on gyrotactic microorganism are mentioned in [34, 35].

For the exploration and optimization of thermal processes, analysis of entropy generation has been widely taken into consideration in recent times. Phenomenon of entropy generation was first explained by Bejan [36]. He reported that entropy generation occurs due to viscous forces and transport of heat in flow of convective fluid. Akmal *et al* [37] investigated the entropy analysis for the squeezing flow of nanofluid under the appliance of hyperbolic heat flux. They considered the effects of magnetic field and Joule heating. Similarity transformation are used to transfigure the governing flow equations into ordinary differential equations. They elucidated the governing equations numerically via Keller box scheme. They found that increasing values of magnetic parameter reduces the fluid velocity but increases the fluid temperature and system entropy. Dalir [38] analyzed the entropy generation for the forced convection laminar flow of Jeffrey fluid over an isothermal impermeable sheet numerically. He described that mounting values of Brinkman number and Reynold's number increases the Bejan number. Shojaeian and Kosar [39] analytically studied the analysis of entropy generation with isothermal conditions between parallel plates. They depicted that the entropy generation

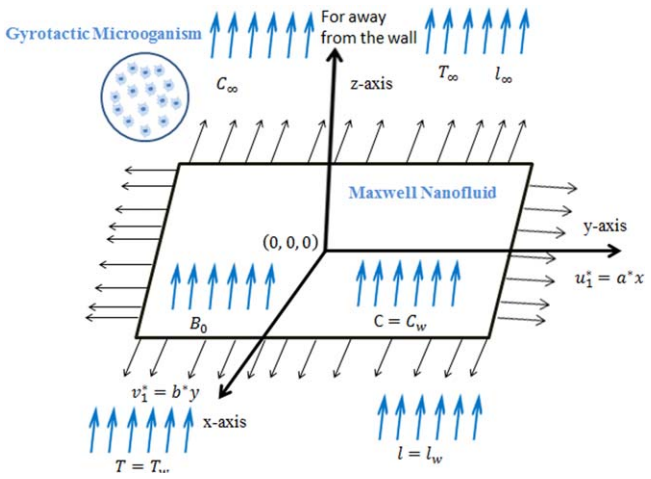

Figure 1. Geometry of the problem.

increases significantly for shear thickening fluids and entropy reduces with slip conditions. Some recent literature covering the entropy generation and magnetic field effects under different flow considerations are mentioned in [40–44].

The novelty of the present work contains the mechanism of thermal radiation, heat generation/absorption with the addition of hyperbolic heat and mass fluxes and also the consideration of homogeneous–heterogeneous reactions with the entropy generation makes the problem attractive for the researches in the field of fluid dynamics. To the best of authors knowledge, these effects for Maxwell model has been not reported by any researcher yet. Present research fills this huge gap in the existing literature. System of transformed modeled expressions are solved via OHAM [45–47]. The impact of numerous fluid flow parameters on obtained solution is discussed with the help of graphs.

2. Mathematical description and flow field analysis

Boundary layer flow of Maxwell nanoliquid containing gyrotactic microorganism over a linear stretched surface under the transport phenomenon of heat and mass is considered in this work. Involvement of thermal radiations and heat source/sink are also considered. Cartesian coordinate system is adopted in such a fashion that surface is coextensive with xy-plane and fluid flow occupies the region where $z \geqslant 0$. Magnetic field $\mathbf{B} = [0,\ 0,\ B_0]$ is applied normal to the stretched surface and the impact of Hall current is insignificant due to small magnetic Reynolds number. Cattaneo–Christov theory is used to describe the transport of mass and heat and the governing laws are presented by using the prevailing boundary layer analysis and the flow situation are shown in figure 1 and boundary layer equations are as follows

$$\frac{\partial u_1^*}{\partial x} + \frac{\partial v_1^*}{\partial y} + \frac{\partial w_1^*}{\partial z} = 0, \tag{1}$$

$$\begin{aligned} u_1^*\frac{\partial u_1^*}{\partial x} + v_1^*\frac{\partial u_1^*}{\partial y} + w_1^*\frac{\partial u_1^*}{\partial z} &= \frac{g_a}{\rho_f}[\rho_f\beta_a(1-C_\infty) \\ &\times (T-T_\infty) - (\rho_p-\rho_\infty)(C-C_\infty) - \gamma(\rho_l-\rho_\infty) \\ &\times (l-l_\infty)] \\ &+ \nu_1\frac{\partial^2 u_1^*}{\partial z^2} - \delta_0\begin{pmatrix}(u_1^*)^2\frac{\partial^2 u_1^*}{\partial x^2} + (v_1^*)^2\frac{\partial^2 u_1^*}{\partial y^2} \\ + (w_1^*)^2\frac{\partial^2 u_1^*}{\partial z^2} + 2u_1^*v_1^*\frac{\partial^2 u_1^*}{\partial x\partial y} \\ + 2v_1^*w_1^*\frac{\partial^2 u_1^*}{\partial z\partial y} + 2u_1^*w_1^*\frac{\partial^2 u_1^*}{\partial z\partial x}\end{pmatrix} - \frac{\sigma_0 B_0^2}{\rho_f} \\ &\times \left(u_1^* + \delta_0 w_1^*\frac{\partial u_1^*}{\partial z}\right), \end{aligned} \tag{2}$$

$$\begin{aligned} u_1^*\frac{\partial v_1^*}{\partial x} + v_1^*\frac{\partial v_1^*}{\partial y} + w_1^*\frac{\partial v_1^*}{\partial z} &= \nu_1\frac{\partial^2 v_1^*}{\partial z^2} \\ &- \delta_0\begin{pmatrix}(u_1^*)^2\frac{\partial^2 v_1^*}{\partial x^2} + (v_1^*)^2\frac{\partial^2 v_1^*}{\partial y^2} \\ + (w_1^*)^2\frac{\partial^2 v_1^*}{\partial z^2} + 2u_1^*v_1^*\frac{\partial^2 v_1^*}{\partial x\partial y} \\ + 2v_1^*w_1^*\frac{\partial^2 v_1^*}{\partial z\partial y} + 2u_1^*w_1^*\frac{\partial^2 v_1^*}{\partial z\partial x}\end{pmatrix} - \frac{\sigma_0 B_0^2}{\rho_f} \\ &\times \left(v_1^* + \delta_0 w_1^*\frac{\partial v_1^*}{\partial z}\right), \end{aligned} \tag{3}$$

$$\begin{aligned} u_1^*\frac{\partial T}{\partial x} + v_1^*\frac{\partial T}{\partial y} + w_1^*\frac{\partial T}{\partial z} &= -\frac{1}{\rho_f c_p}\nabla.\widetilde{\mathbf{Q}} + \frac{Q_a(T-T_\infty)}{\rho_f c_p} \\ &+ \frac{\sigma B_0^2((u_1^*)^2 + (v_1^*)^2)}{\rho_f c_p} - \frac{1}{\rho_f c_p}\frac{\partial \widetilde{\mathbf{Q}}_r}{\partial z} \\ &+ \chi_a\left[a_1\frac{\partial C}{\partial z}\frac{\partial T}{\partial z} + \frac{a_2}{T_\infty}\left(\frac{\partial T}{\partial z}\right)^2\right], \end{aligned} \tag{4}$$

$$u_1^*\frac{\partial C}{\partial x} + v_1^*\frac{\partial C}{\partial y} + w_1^*\frac{\partial C}{\partial z} = -\nabla.\widetilde{\mathbf{J}} + \frac{a_2}{T_\infty}\frac{\partial^2 T}{\partial z^2}, \tag{5}$$

$$u_1^*\frac{\partial A_1^*}{\partial x} + v_1^*\frac{\partial A_1^*}{\partial y} + w_1^*\frac{\partial A_1^*}{\partial z} = \delta_1\frac{\partial^2 A_1^*}{\partial z^2} - \alpha_c^* A_1^*(B_1^*)^2, \tag{6}$$

$$u_1^*\frac{\partial B_1^*}{\partial x} + v_1^*\frac{\partial B_1^*}{\partial y} + w_1^*\frac{\partial B_1^*}{\partial z} = \delta_2\frac{\partial^2 B_1^*}{\partial z^2} + \alpha_c^* A_1^*(B_1^*)^2. \tag{7}$$

$$\begin{aligned} u_1^*\frac{\partial l}{\partial x} + v_1^*\frac{\partial l}{\partial y} + w_1^*\frac{\partial l}{\partial z} + \frac{\xi_c w_0}{\Delta C}\left[l\frac{\partial^2 C}{\partial z^2} + \frac{\partial l}{\partial z}\frac{\partial C}{\partial z}\right] \\ = D_c\frac{\partial^2 l}{\partial z^2}. \end{aligned} \tag{8}$$

Hyperbolic heat flux ($\widetilde{\mathbf{Q}}$) and generalized Fick's law for mass flux ($\widetilde{\mathbf{J}}$) are enunciated as:

$$\widetilde{\mathbf{Q}} + \varepsilon_E\left[\frac{\partial\widetilde{\mathbf{Q}}}{\partial t} + \mathbf{V}.\nabla\widetilde{\mathbf{Q}} - \widetilde{\mathbf{Q}}.\nabla\mathbf{V} + (\nabla.\mathbf{V})\widetilde{\mathbf{Q}}\right] = -K_a\nabla.T, \tag{9}$$

$$\widetilde{\mathbf{J}} + \varepsilon_C\left[\frac{\partial\widetilde{\mathbf{J}}}{\partial t} + \mathbf{V}.\nabla\widetilde{\mathbf{J}} - \widetilde{\mathbf{J}}.\nabla\mathbf{V} + (\nabla.\mathbf{V})\widetilde{\mathbf{J}}\right] = -D_a\nabla.C. \tag{10}$$

Using the assumptions of incompressibility and steady state, equations (9)–(10) reduces to the following form:

$$\widetilde{\mathbf{Q}} + \varepsilon_E[\mathbf{V}.\nabla\widetilde{\mathbf{Q}} - \widetilde{\mathbf{Q}}.\nabla\mathbf{V}] = -K_a\nabla.T, \tag{11}$$

$$\widetilde{\mathbf{J}} + \varepsilon_C[\mathbf{V}.\nabla\widetilde{\mathbf{J}} - \widetilde{\mathbf{J}}.\nabla\mathbf{V}] = -D_a\nabla.C. \tag{12}$$

For $\varepsilon_E = \varepsilon_C = 0$, equations (11)–(12) shrinks to traditional Fourier's law of heat conduction and Fick's 2nd laws respectively. Eliminating heat flux ($\widetilde{\mathbf{Q}}$) between equations (4) and (11) and mass flux ($\widetilde{\mathbf{J}}$) between equations (5) and (12), we achieve the following equations for heat and mass transposition:

$$\begin{aligned} u_1^*\frac{\partial T}{\partial x} + v_1^*\frac{\partial T}{\partial y} + w_1^*\frac{\partial T}{\partial z} + A^* &= \frac{K_a}{\rho_f c_p}\frac{\partial^2 T}{\partial z^2} \\ &+ \frac{\sigma_0 B_0^2((u_1^*)^2 + (v_1^*)^2)}{\rho_f c_p} + \frac{Q_a(T - T_\infty)}{\rho_f c_p} \\ &- \frac{1}{\rho_f c_p}\frac{\partial\widetilde{\mathbf{Q}}_r}{\partial z} + \chi_a\left[a_1\frac{\partial C}{\partial z}\frac{\partial T}{\partial z} + \frac{a_2}{T_\infty}\left(\frac{\partial T}{\partial z}\right)^2\right], \end{aligned} \tag{13}$$

$$u_1^*\frac{\partial C}{\partial x} + v_1^*\frac{\partial C}{\partial y} + w_1^*\frac{\partial C}{\partial z} + B^* = D_a\frac{\partial^2 C}{\partial z^2} + \frac{a_2}{T_\infty}\frac{\partial^2 T}{\partial z^2}, \tag{14}$$

where

$$\begin{aligned} A^* &= A_1^* + A_2^* + A_3^*, \\ A_1^* &= (u_1^*)^2\frac{\partial^2 T}{\partial x^2} + (v_1^*)^2\frac{\partial^2 T}{\partial y^2} + (w_1^*)^2\frac{\partial^2 T}{\partial z^2} \\ &\quad + u_1^*\frac{\partial u_1^*}{\partial x}\frac{\partial T}{\partial x} + v_1^*\frac{\partial u_1^*}{\partial y}\frac{\partial T}{\partial x}, \\ A_2^* &= w_1^*\frac{\partial u_1^*}{\partial z}\frac{\partial T}{\partial x} + u_1^*\frac{\partial v_1^*}{\partial x}\frac{\partial T}{\partial y} + v_1^*\frac{\partial v_1^*}{\partial y}\frac{\partial T}{\partial y} \\ &\quad + w_1^*\frac{\partial v_1^*}{\partial y}\frac{\partial T}{\partial y} + u_1^*\frac{\partial w_1^*}{\partial x}\frac{\partial T}{\partial z}, \\ A_3^* &= v_1^*\frac{\partial w_1^*}{\partial y}\frac{\partial T}{\partial z} + w_1^*\frac{\partial w_1^*}{\partial z}\frac{\partial T}{\partial z} + 2u_1^*v_1^*\frac{\partial^2 T}{\partial x\partial y} \\ &\quad + 2v_1^*w_1^*\frac{\partial^2 T}{\partial z\partial y} + 2u_1^*w_1^*\frac{\partial^2 T}{\partial x\partial z}, \end{aligned} \tag{15}$$

and

$$\begin{aligned} B^* &= B_1^* + B_2^* + B_3^*, \\ B_1^* &= (u_1^*)^2\frac{\partial^2 C}{\partial x^2} + (v_1^*)^2\frac{\partial^2 C}{\partial y^2} + (w_1^*)^2\frac{\partial^2 C}{\partial z^2} + u_1^*\frac{\partial u_1^*}{\partial x} \\ &\quad \times \frac{\partial C}{\partial x} + v_1^*\frac{\partial u_1^*}{\partial y}\frac{\partial C}{\partial x}, \\ B_2^* &= w_1\frac{\partial u_1^*}{\partial z}\frac{\partial C}{\partial x} + u_1^*\frac{\partial v_1^*}{\partial x}\frac{\partial C}{\partial y} + v_1^*\frac{\partial v_1^*}{\partial y}\frac{\partial C}{\partial y} + w_1^*\frac{\partial v_1^*}{\partial y} \\ &\quad \times \frac{\partial C}{\partial y} + u_1^*\frac{\partial w_1^*}{\partial x}\frac{\partial C}{\partial z}, \\ B_3^* &= v_1^*\frac{\partial w_1^*}{\partial y}\frac{\partial C}{\partial z} + w_1^*\frac{\partial w_1^*}{\partial z}\frac{\partial C}{\partial z} + 2u_1^*v_1^*\frac{\partial^2 C}{\partial x\partial y} + 2v_1^*w_1^* \\ &\quad \times \frac{\partial^2 C}{\partial z\partial y} + 2u_1^*w_1^*\frac{\partial^2 C}{\partial x\partial z}. \end{aligned} \tag{16}$$

Boundary conditions in dimensional form are given as

$$\begin{cases} u_1^* = a^*x,\ v_1^* = b^*y,\ w_1^* = 0, \\ T = T_w,\ C = C_w,\ l = l_w, \\ \delta_1\dfrac{\partial A_1^*}{\partial z} = N_s A_1^*, \\ \delta_2\dfrac{\partial B_1^*}{\partial z} = -N_s B_1^* \text{at} z = 0, \\ u_1^* \to 0,\ v_1^* \to 0,\ C \to C_\infty,\ T \to T_\infty, \\ A_1^* \to A_0^*,\ l \to 0, \\ B_1^* \to 0 \text{as} z \to \infty. \end{cases} \tag{17}$$

Introducing the subsequent transfigurations for the convoluted physical quantities

$$\begin{cases} u_1^* = a^*xf'(\xi),\ v_1^* = b^*yg'(\xi),\ w_1^* = -\sqrt{a^*\nu_1}(f(\xi) \\ \qquad + g(\xi)),\ A_1^* = A_0^*r(\xi),\ B_1^* = A_0^*h(\xi), \\ \xi = \sqrt{\dfrac{a^*}{\nu_1}}z,\ \theta(\xi) = \dfrac{T - T_\infty}{T_w - T_\infty},\ \varphi(\xi) = \dfrac{C - C_\infty}{C_w - C_\infty},\ R(\zeta) \\ \quad = \dfrac{l - l_\infty}{l_w - l_\infty}. \end{cases} \tag{18}$$

Exploiting the above declared renovations, mass conservation equation is identically satisfied and rest of the equations including momentum, energy, mass transfer, and gyrotactic microorganism reduce to the following system of coupled nonlinear ordinary differential equations

$$\begin{aligned} &f''' - (M^2D_1 + 1)(f + g)f'' - (f')^2 \\ &\quad + \delta_m[\theta - Br\varphi - RaR] - M^2f' \\ &\quad + D_1[2(f + g)f''f' - (f + g)^2f'''] = 0, \end{aligned} \tag{19}$$

$$\begin{aligned} &g''' - (M^2D_1 + 1)(f + g)g'' - (g')^2 + D_1[2(f + g)g''g' \\ &\quad - (f + g)^2g'''] - M^2g' = 0, \end{aligned} \tag{20}$$

Table 1. Convergence examination of established series solutions.

a	$\hat{E}_k^{*f}$	$\hat{E}_k^{*g}$	$\hat{E}_k^{*\theta}$	$\hat{E}_k^{*\varphi}$	$\hat{E}_k^{*r}$	$\hat{E}_k^{*R}$
2	3.036×10^{-2}	1.192×10^{-2}	1.937×10^{-2}	1.317×10^{-2}	1.294×10^{-2}	2.728×10^{-2}
4	2.248×10^{-4}	2.925×10^{-3}	1.193×10^{-3}	1.294×10^{-3}	1.174×10^{-3}	3.613×10^{-3}
6	3.621×10^{-6}	1.813×10^{-4}	3.419×10^{-4}	1.395×10^{-4}	2.739×10^{-4}	2.839×10^{-4}
8	5.054×10^{-7}	3.207×10^{-5}	1.715×10^{-6}	1.283×10^{-5}	1.451×10^{-5}	4.714×10^{-5}
10	2.913×10^{-7}	1.253×10^{-6}	4.205×10^{-7}	2.638×10^{-6}	5.729×10^{-6}	5.937×10^{-6}
12	4.022×10^{-8}	1.138×10^{-8}	2.403×10^{-8}	1.763×10^{-7}	1.502×10^{-6}	7.827×10^{-6}
16	2.916×10^{-9}	2.162×10^{-9}	5.927×10^{-9}	7.395×10^{-8}	1.623×10^{-7}	3.726×10^{-7}
20	1.104×10^{-11}	3.571×10^{-10}	1.924×10^{-9}	4.163×10^{-8}	1.539×10^{-8}	2.427×10^{-8}

$$\frac{1}{\mathrm{Pr}}\left(1+\frac{4}{3}\chi_R\right)\theta'' + (f+g)\theta' - \lambda_1(f+g)[(f'+g')\theta' + (f+g)\theta''] + M^2Ec[(f')^2+(g')^2] + \chi_H\theta + \chi_B\theta'\varphi' + \chi_T(\theta')^2 = 0, \tag{21}$$

$$\frac{1}{Sc}\varphi'' + (f+g)\varphi' - \lambda_2(f+g)[(f'+g')\varphi' + (f+g)\varphi''] + \frac{\chi_T}{\chi_B}\frac{1}{Sc}\theta'' = 0, \tag{22}$$

$$\frac{1}{Sr}r'' + (f+g)r' - k_1 r(1-r)^2 = 0, \tag{23}$$

$$R'' + L_1(f+g)R' - L_1Rf' - P_1[R'\varphi' + (R+\Omega_1)\varphi''] = 0. \tag{24}$$

Transformed conditions for equations (19)–(24) are

$$\begin{cases} f=0,\ f'=1,\ g=0,\ g'=\beta_1,\ \theta=1,\ \varphi=1,\ r'=N_s r, \\ R=1 \text{ at } \xi=0, \\ f'\to 0,\ g'\to 0,\ \theta\to 0,\ \varphi\to 0,\ r\to 1,\ R\to 0 \text{ as} \\ \xi\to\infty. \end{cases} \tag{25}$$

3. Entropy generation investigation

Relation for the entropy generation for Maxwell nanofluid is considered as:

$$E_G = \underbrace{\frac{K_a}{T_\infty^2}\left[1+\frac{16\sigma T_\infty^3}{3K_a k^{**}}\right]\left(\frac{\partial T}{\partial z}\right)^2}_{} + \underbrace{\frac{R_D}{C_\infty}\left(\frac{\partial C}{\partial z}\right)^2 + \frac{R_D}{T_\infty}\left(\frac{\partial C}{\partial z}\right)\left(\frac{\partial T}{\partial z}\right)}_{} + \underbrace{\frac{\sigma}{T_\infty}B_0^2[((u_1^*)^2+(v_1^*)^2)]}_{}, \tag{26}$$

Equation (26) contains three terms namely thermal irreversibility, Joule heating irreversibility and concentration irreversibility. The dimensionless form of entropy generation is expressed as:

$$E_G = (1+\chi_R)(\theta')^2(\varepsilon_1)^2 + MBr\varepsilon_1[(f')^2+(g')^2] + \varepsilon_3\varepsilon_2(\varphi')^2 + \varepsilon_3\varepsilon_1\theta'\varphi'. \tag{27}$$

4. Solution via OHAM

Many analytical and numerical schemes are used to compute the solution of governing coupled system of fluid flow problems. Here we, suggest the optimal homotopic scheme proposed by Liao [47], which needs no discretization and small parameters assumption like the numerical and perturbation approaches. Moreover, the proposed algorithm deals the linear and nonlinear problem in a similar fashion and there is no requirement of Lagrange multiplier which is used in variational scheme which overcomes the successive integral operators. Initial estimates for dimensionless velocities, temperature and concentration fields corresponding to linear operators are

$$f_0 = 1-\frac{1}{e^\xi},\ g_0 = \beta_1\left(1-\frac{1}{e^\xi}\right),\ \theta_0 = \frac{1}{e^\xi},\ \varphi_0 = \frac{1}{e^\xi},\ r_0 = 1-\frac{1}{2}e^{-N_s\xi},\ R_0 = \frac{1}{e^\xi}, \tag{28}$$

$$l_1 = (m^3-m),\ l_2 = (m^3-m),\ l_3 = (m^2-1),\ l_4 = (m^2-1),\ l_5 = (m^2-1),\ l_6 = (m^2-1), \tag{29}$$

these linear operators conform the following features

$$\begin{cases} l_1[\alpha_1^* + \alpha_2^* e^\xi + \alpha_3^* e^{-\xi}] = 0,\ l_2[\alpha_4^* + \alpha_5^* e^\xi + \alpha_6^* e^{-\xi}] = 0, \\ l_3[\alpha_7^* e^\xi + \alpha_8^* e^{-\xi}] = 0, \\ l_4[\alpha_9^* e^\xi + \alpha_{10}^* e^{-\xi}] = 0,\ l_5[\alpha_{11}^* e^\xi + \alpha_{12}^* e^{-\xi}] = 0, \\ l_6[\alpha_{13}^* e^\xi + \alpha_{14}^* e^{-\xi}] = 0, \end{cases} \tag{30}$$

where $\alpha_i^*(i=1-14)$ are the indiscriminate constants.

5. Optimal convergence constraint parameter

This portion addresses the idea of minimization of average squared residuals errors which regulate the convergence zone and homotopic solutions. A case of such reduction in error is displayed in table 1, which is manipulated by **BVPh 2.0.** Table 1 presents that for higher order deformations, error reduces which

Table 2. Comparative analysis of $-f''(0)$ and $-g''(0)$ for $M = \varepsilon = 0$.

	Present results		Ammar *et al* [48]		Wang [49]		Liu and Andersson [50]	
β_1	$-f''(0)$	$-g''(0)$	$-f''(0)$	$-g''(0)$	$-f''(0)$	$-g''(0)$	$-f''(0)$	$-g''(0)$
0.0	1.0	0.0	1.0	0.0	1.0	0.0	1.0	0.0
0.25	1.048810	0.194562	1.048811	0.194564	1.048813	0.194564	1.048813	0.194565
0.50	1.093096	0.465204	1.093095	0.465205	1.093097	0.465205	1.093096	0.465206
0.75	1.134482	0.794620	1.134486	0.794618	1.134486	0.794622	1.134486	0.794619
1.0	1.173719	1.173719	1.173721	1.173721	1.173720	1.173720	1.173721	1.173721

confirm the convergence of homotopic solution.

$$
\begin{cases}
\hat{E}_b^{*f} = \dfrac{1}{a+1}\displaystyle\sum_{s=0}^{a}\left[N_f\left(\sum_{a^*=0}^{b} f^*(\xi),\ \sum_{a^*=0}^{b} g^*(\xi),\ \sum_{a^*=0}^{b} \theta^*(\xi),\ \sum_{a^*=0}^{b} \varphi^*(\xi),\ \sum_{a^*=0}^{b} R^*(\xi)\right)_{\xi=s\delta\xi}\right]^2,\\
\hat{E}_b^{*g} = \dfrac{1}{a+1}\displaystyle\sum_{s=0}^{a}\left[N_f\left(\sum_{a^*=0}^{b} f^*(\xi),\ \sum_{a^*=0}^{b} g^*(\xi)\right)_{\xi=s\delta\xi}\right]^2,\\
\hat{E}_b^{*\theta} = \dfrac{1}{a+1}\displaystyle\sum_{s=0}^{a}\left[N_\theta\left(\sum_{a^*=0}^{b} f^*(\xi),\ \sum_{a^*=0}^{b} g^*(\xi),\ \sum_{a^*=0}^{b} \theta^*(\xi),\ \sum_{a^*=0}^{b} \varphi^*(\xi)\right)_{\xi=s\delta\xi}\right]^2,\\
\hat{E}_b^{*\varphi} = \dfrac{1}{a+1}\displaystyle\sum_{a}^{s=0}\left[N_\varphi\left(\sum_{a^*=0}^{b} f^*(\xi),\ \sum_{a^*=0}^{b} g^*(\xi),\ \sum_{a^*=0}^{b} \varphi^*(\xi),\ \sum_{b}^{a^*=0} \theta^*(\xi)\right)_{\xi=s\delta\xi}\right]^2,\\
\hat{E}_b^{*r} = \dfrac{1}{a+1}\displaystyle\sum_{s=0}^{a}\left[N_r\left(\sum_{b}^{a^*=0} f^*(\xi),\ \sum_{b}^{a^*=0} g^*(\xi),\ \sum_{b}^{a^*=0} r^*(\xi)\right)_{\xi=s\delta\xi}\right]^2,\\
\hat{E}_b^{*R} = \dfrac{1}{a+1}\displaystyle\sum_{s=0}^{a}\left[N_R\left(\sum_{a^*=0}^{b} f^*(\xi),\ \sum_{a^*=0}^{b} g^*(\xi),\ \sum_{a^*=0}^{b} \varphi^*(\xi),\ \sum_{a^*=0}^{b} R^*(\xi)\right)_{\xi=s\delta\xi}\right]^2,
\end{cases}
\tag{31}
$$

$$
\hat{E}_b^{*\text{total}} = \hat{E}_b^{*f} + \hat{E}_b^{*g} + \hat{E}_b^{*\theta} + \hat{E}_b^{*\varphi} + \hat{E}_b^{*r} + \hat{E}_b^{*R}. \tag{32}
$$

6. Graphical results and solution analysis

This portion contains the analysis of obtained solution. The involvement of different emerging parameters on computed solutions is displayed and conferred through figures 2–18.

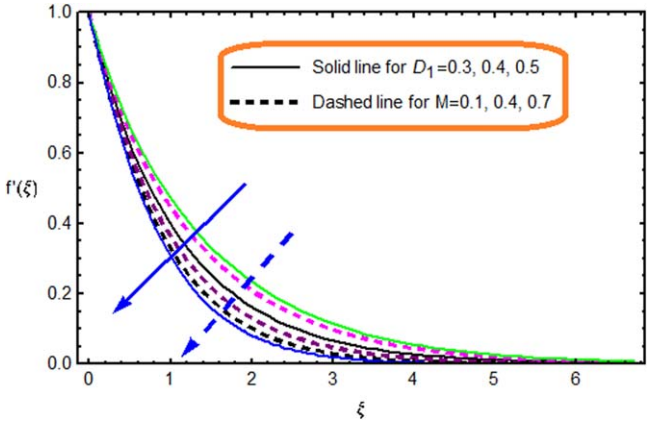

Figure 2. Influence of D_1 and M on $f'(\xi)$.

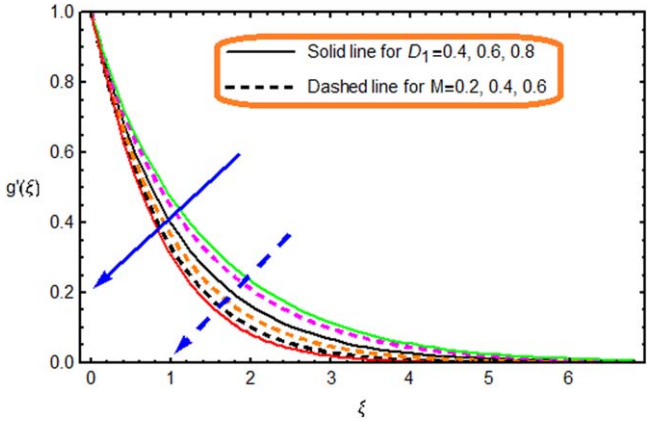

Figure 3. Influence of D_1 and M on $g'(\xi)$.

Table 2 is prepared in order to study the comparative analysis of achieved solutions with the reported studies in the open literature, as a limiting case of present investigation. We have found that, our results are in good agreement with the previous findings. Figures 2–3 are demonstrated to notice the combine bearing of magnetic parameter (M) and non-dimensional fluid relaxation time (D_1) on fluid velocities $f'(\xi)$ and $g'(\xi)$ and hydrodynamic boundary layer. Their combine enactment perceived that fluid velocity decreases for higher values of these influential parameters. Since (D_1) is defined to be the time taken by moving fluid in order to obtain equilibrium in response of applied stress. Moreover, physically with smaller (D_1) materials shows liquid like behavior and higher values of (D_1) corresponds to establish the behavior of solid like materials. The velocity profiles are slanted towards

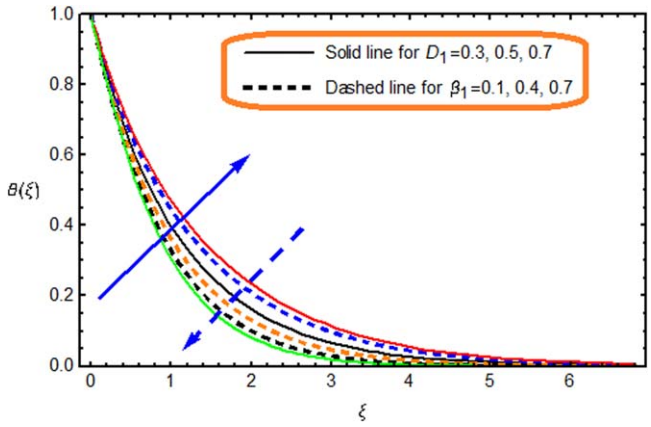

Figure 4. Influence of D_1 and β_1 on $\theta(\xi)$.

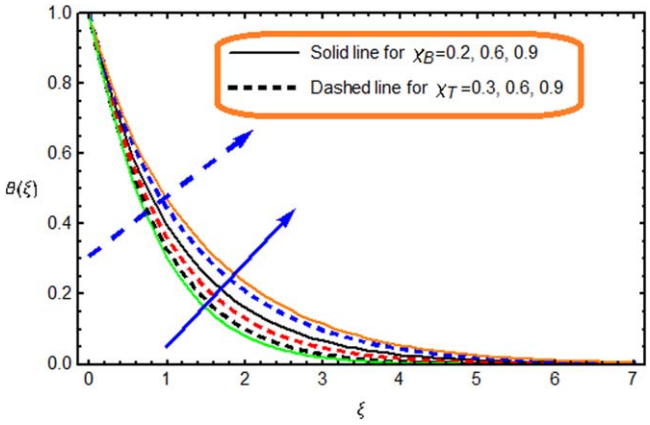

Figure 7. Influence of χ_B and χ_T on $\theta(\xi)$.

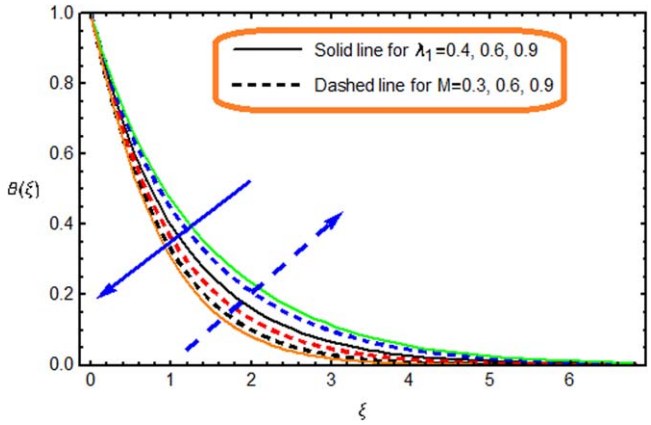

Figure 5. Influence of λ_1 and M on $\theta(\xi)$.

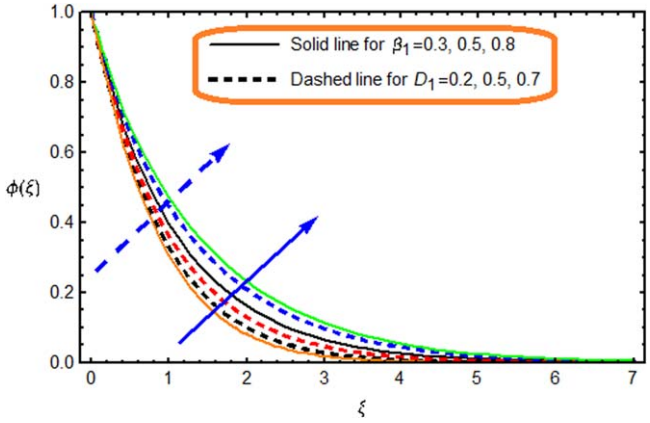

Figure 8. Influence of D_1 and β_1 on $\phi(\xi)$.

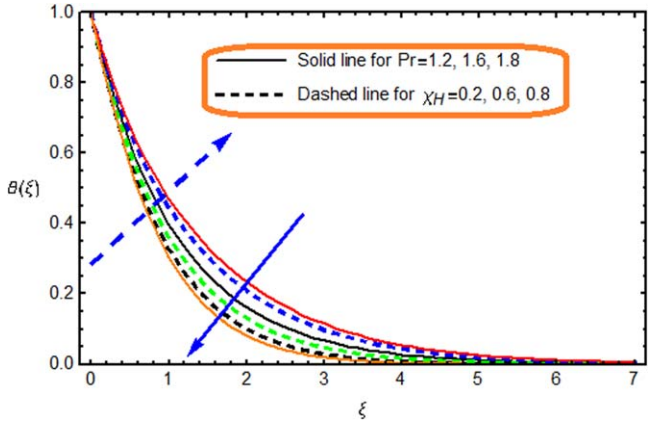

Figure 6. Influence of Pr and χ_H on $\theta(\xi)$.

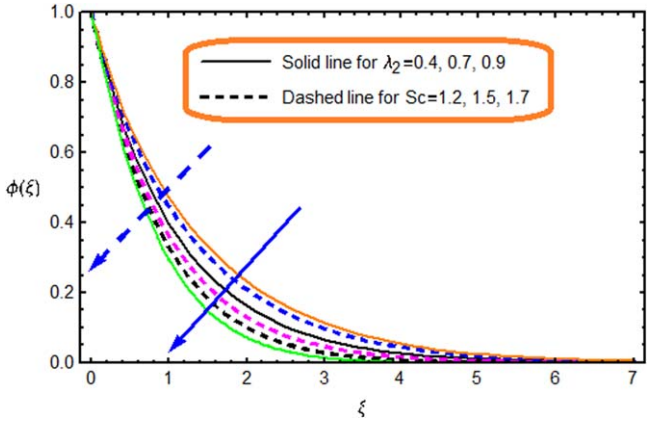

Figure 9. Influence of λ_2 and Sc on $\phi(\xi)$.

the wall when (D_1) is augmented which designate that fluid velocity and associated layer wideness are diminishing function of (D_1). The impact of magnetic parameter (M) on fluid velocities $f'(\xi)$ and $g'(\xi)$ is also presented in figures 2–3. Magnetic parameter appears in the equation of motion for fluid flow due to the consideration of conduction in fluids. This consideration controls the turbulence in the fluid flow. Since turbulence is controlled due to increasing the magnetic effect, which shows the decline in the fluid velocity. Moreover, magnetic effect links the appliance of Lorentz force, which is resistive in nature and as a result, decline in fluid velocity is noticed. Also, due to Lorentz force, high resistance between the molecules of fluid occurs which results in declination in the velocity field.

Figure 4 is designed to analyze that how temperature $\theta(\xi)$ gets exaggerated with the discrepancy of ratio parameter (β_1) and fluid relaxation time (D_1). It is depicted that fluid temperature decreases due to negligible resistance by growing (β_1)

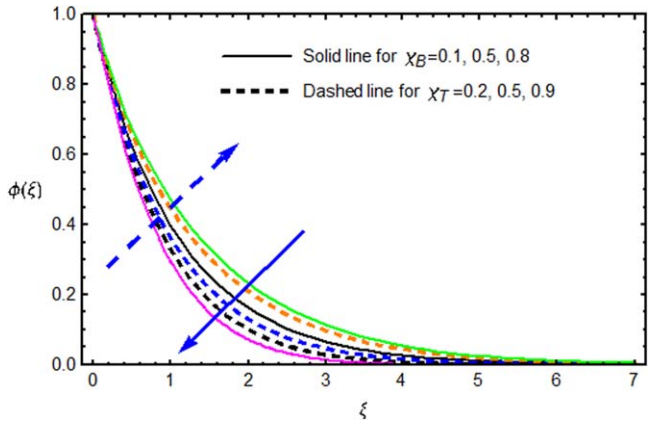

Figure 10. Influence of χ_B and χ_T on $\phi(\xi)$.

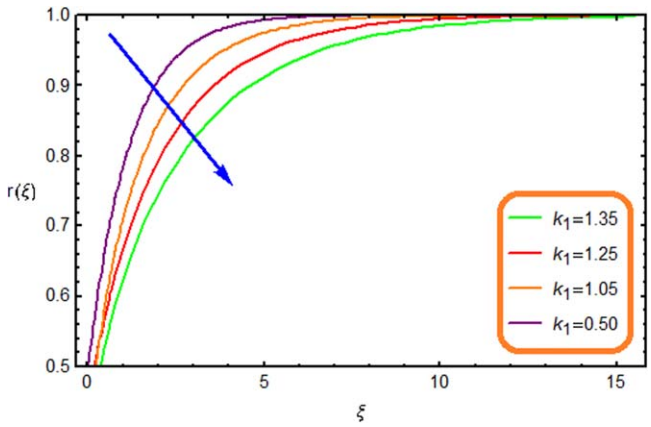

Figure 11. Influence of k_1 on $r(\xi)$.

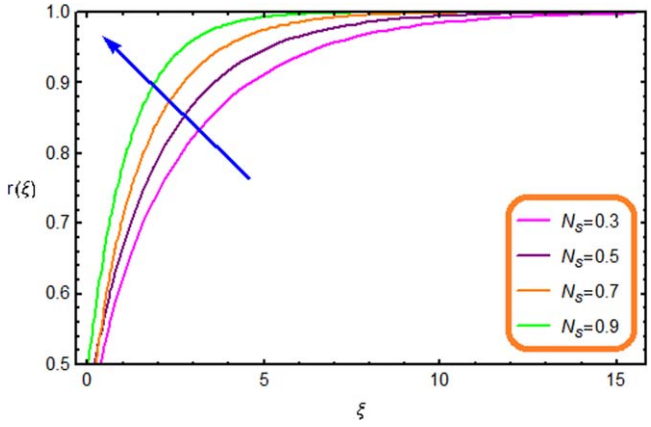

Figure 12. Influence of N_s on $r(\xi)$.

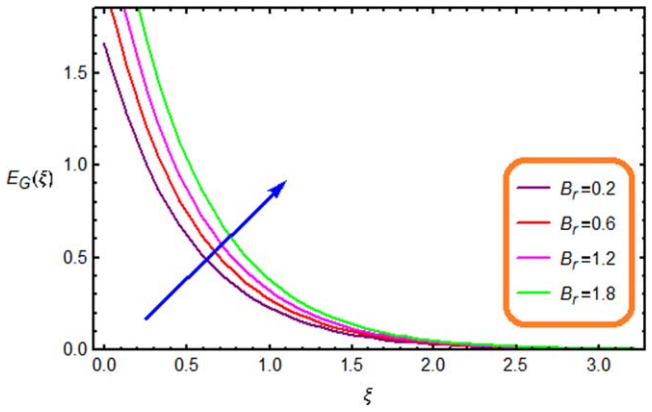

Figure 13. Influence of B_r on $E_G(\xi)$.

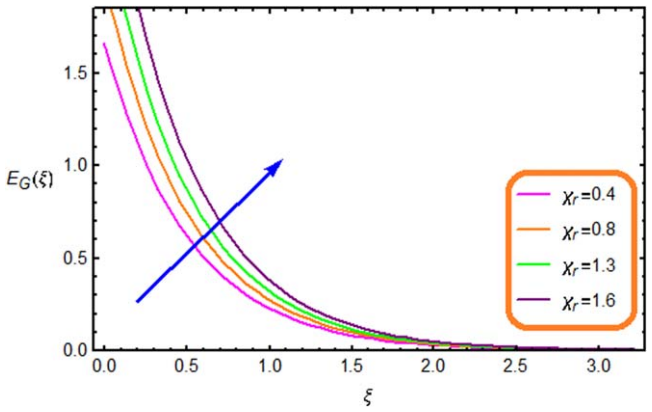

Figure 14. Influence of χ_r on $E_G(\xi)$.

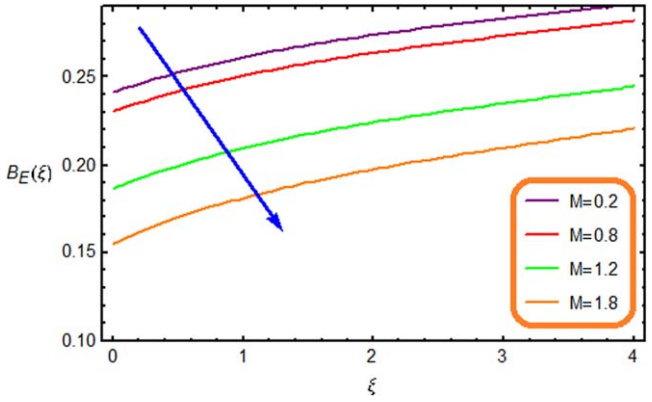

Figure 15. Influence of M on $B_E(\xi)$.

and a significantly rise in it is observed for mounting values of fluid relaxation time (D_1). Increasing values of fluid relaxation time (D_1) corresponds that friction is produced in the fluid which cause to rise in fluid temperature. Figure 5 is plotted for $\theta(\xi)$ against the mounting values of thermal relaxation parameter (λ_1) and magnetic parameter (M). It is perceived that $\theta(\xi)$ decelerates by growing thermal relaxation parameter (λ_1). Physically, larger (λ_1) describes that heating process in fluid flow lessens, which cools down the fluid and as a result, fluid temperature decreases and also it tells that due to increase in thermal relaxation time heated particles of fluid requires more time transfer energy to their connected neighboring fluid particles due to which system temperature falls down. Increase in (M) shows the involvement of strong resistive force due to which the heated particles of fluid offers more resistance and due to this temperature of the fluid increases. Also, due to escalating values of magnetic parameter, strong Lorentz force is experienced between the

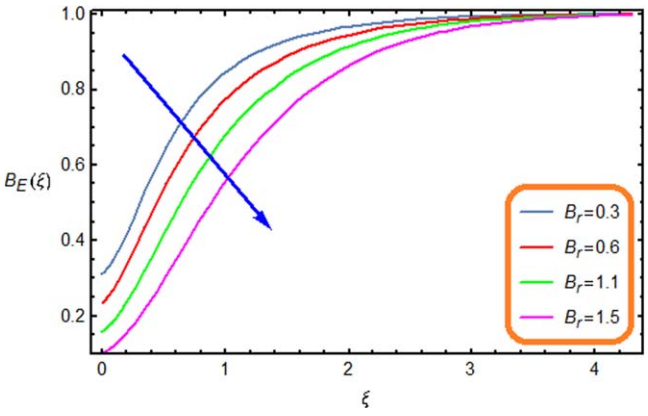

Figure 16. Influence of B_r on $B_E(\xi)$.

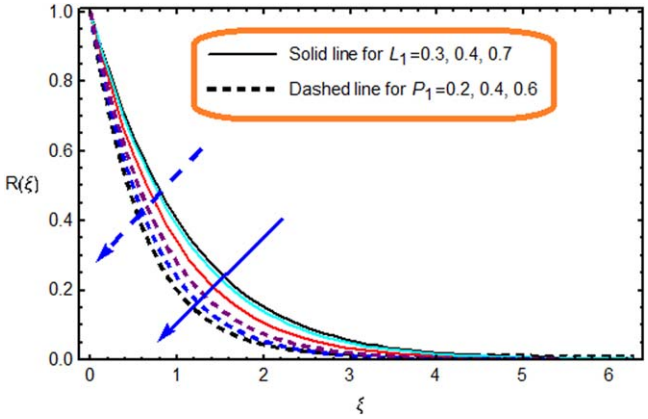

Figure 17. Influence of L_1 and P_1 on $R(\xi)$.

molecules of fluid and more friction occurs between the fluid particles which results in enhancement in the temperature field. Figure 6 is prepared to measure the combine involvement of Prandtl number (Pr) and the heat source/sink parameter (χ_H) on temperature. Since Prandtl number (Pr) explains about fluid category and about the wideness of thermal and hydrodynamic boundary layer. It has been observed that by increasing Prandtl number (Pr), thermal diffusion is much less than the momentum diffusion and due to this non-dimensional temperature $\theta(\xi)$ and connected layer thickness reduces. Also, higher values of Prandtl number (Pr) shows that heated fluid particles travels slowly towards the cold region from hot. Figure 6 also exhibits the impression of heat generation parameter ($\chi_H > 0$) on $\theta(\xi)$. It is noticed that an upturn in (χ_H) upsurges the temperature field. When ($\chi_H > 0$) is increased, more heat is produced in the fluid that causes higher temperature and stronger thermal boundary layer wideness. Figure 7 shows the combined inspiration of thermophoresis parameter (χ_T) and Brownian motion parameter (χ_B) on temperature $\theta(\xi)$. Higher values of (χ_T) produces a larger temperature field due to the thermal transport within the boundary layer. Figure 7 also shows the impact of (χ_B) on $\theta(\xi)$. It is plotted to notify the involvement of (χ_B) on temperature. It demonstrates that due to increase in (χ_B) more heat is produced within the fluid particles. As a result temperature field upsurges.

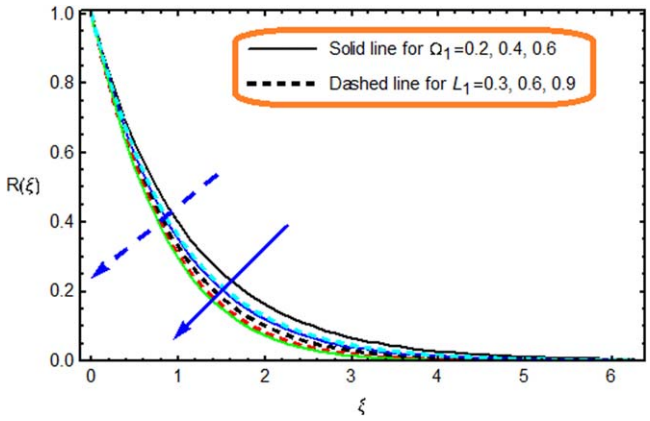

Figure 18. Influence of L_1 and Ω_1 on $R(\xi)$.

Figure 8 is drafted to notice the combine bearing of ratio parameter (β_1) and fluid relaxation parameter (D_1) on fluid concentration $\varphi(\xi)$. It portrays that ratio parameter (β_1) and fluid relaxation parameter (D_1) are directly related to $\varphi(\xi)$. Impact of concentration relaxation parameter (λ_2) and Schmidt number (Sc) on concentration profile $\varphi(\xi)$ is presented in figure 9. It shows that (λ_2) is inversely related to $\varphi(\xi)$. Physically, increase in (λ_2) tells us that fluid particles requires more time to transfer mass to the neighboring particles due to which concentration field lessens. Figure 9 is also planned to notice the inspiration of Schmidt number (Sc) on concentration $\varphi(\xi)$. Since Schmidt number (Sc) is the dimensionless number which is the ratio between momentum and mass diffusion and also it tells us about the momentum and concentration boundary layers. Larger (Sc) produces weaker mass diffusion due to which concentration field diminishes. Figure 10 is drafted to observe the involvement of Brownian motion parameter (χ_B) on fluid concentration. It depicts that the concentration of nanofluid reduced with an increase in (χ_B). Furthermore, figure 10 is also prepared to measure the bearing of (χ_T) on concentration. It is detected that $\varphi(\xi)$ varies directly with an increase in (χ_T). Figure 11 presents the comportment of (k_1) on $r(\xi)$. It shows that (k_1) reduces $r(\xi)$. Figure 12 is conscripted to notice the bearing of (Ns) on $r(\xi)$. It depicts that $r(\xi)$ is in direct relation with (Ns). Figure 13 explains the influence of (B_r) on $E_G(\xi)$. It shows that $E_G(\xi)$ upsurges for larger values of Brinkman number. Since Brinkman number (B_r) is defined to be the ratio of heat transfer by conduction to heat produced by viscous heating. Due to increase in Brinkman number (B_r) higher amount of heat is engendered in the system which augments disorderliness of the system and as a result $E_G(\xi)$ boosts up. Figure 14 is plotted to inspect the involvement of (χ_R) on $E_G(\xi)$. It is perceived that $E_G(\xi)$ boosts for larger (χ_R). It is worth mentioning that due to larger (χ_R), more disorderliness occurs. Figure 15 explains the bearing of (M) on $B_E(\xi)$. It depicts that an increase in (M) corresponds to decay in $B_E(\xi)$. Figure 16 is plotted to measure the inspiration of (B_r) on $B_E(\xi)$. It is perceived that mounting values of (B_r) diminishes $B_E(\xi)$. Figure 17 delineates the bearing of bio convection Lewis (L_1) and Peclet numbers (P_1) on density of motile microorganisms $R(\xi)$. Increase in (L_1) and (P_1) corresponds to

decrease in the diffusion of microorganisms and as a result $R(\xi)$ decreases. Figure 18 elucidates that increasing values of concentration difference parameter (Ω_1) has the same impact like (L_1) and (P_1) on $R(\xi)$.

7. Summary of main observations

From the performed exploration, the key findings are listed as

- Velocity field diminishes for larger fluid relaxation parameter and magnetic parameter.
- Augmentation in Schmidt and Prandtl numbers lessens the concentration and temperature fields.
- Increasing values of thermal and concentration relaxation parameters reduces the temperature and concentration fields.
- Temperature field upsurges for mounting values of heat generation parameter.
- Bearing of (β_1) and (D_1) on species profile is opposite to that of solutal relaxation parameter and Schmidt number.
- Similar and contrasting comportment of temperature and concentration is discerned for (χ_T) and (χ_B).
- Higher values of ratio parameter boosts the dimensionless temperature.
- Impact of (β_1) and (D_1) on temperature field is opposite to that of (λ_1) and Prandtl number (Pr).
- Thermal and concentration boundary layers decreases for the higher values of Prandtl and Schmidt numbers.
- Reaction of concentration is larger for (Ns) and it lessens for (k_1).
- Entropy generation upsurges for (χ_r) and (B_r), whereas, magnetic parameter decreases the Bejan number.
- Large values of (L_1), (Ω_1) and (P_1) has the similar impact on $R(\xi)$.

Acknowledgments

R Naz is thankful to the Higher Education Commission (HEC) of Pakistan for the financial support through National Research Program for Universities 2014 (Project number 4090).

ORCID iDs

M Sohail https://orcid.org/0000-0002-1490-0339
Sara I Abdelsalam https://orcid.org/0000-0002-6434-8319

References

[1] Bird R B, Armstrong R C and Hassager O 1987 Dynamics of polymeric liquids *Fluid Mechanics* vol 1 2nd edn (Amsterdam: North-Holland)
[2] Bohme G 1987 Non-Newtonian *Fluid Mechanics* vol 1 2nd edn (Amsterdam: North-Holland)
[3] Joseph D D 1990 *Fluid Dynamics of Visco Elastic Liquids* (New York: Springer)
[4] Elkoumy S R, Barakat E I and Abdelsalam S I 2013 Hall and transverse magnetic field effects on peristaltic flow of a Maxwell fluid through a porous medium, global *J. Pure Appl. Math.* **9** 187–203
[5] Mekheimer K S, Elkomy S R and Abdelsalam S I 2013 Simultaneous effects of magnetic field and space porosity on compressible Maxwell fluid transport induced by a surface acoustic wave in a microchannel *Chin. Phys.* B **22** 124702
[6] Elkoumy S R, Barakat E I and Abdelsalam S I 2012 Hall and porous boundaries effects on peristaltic transport through porous medium of a Maxwell model *Transp. Porous Media* **94** 643–58
[7] Vieru D, Fetecau C and Fetecau C 2008 Flow of a viscoelastic fluid with the fractional Maxwell model between two side walls perpendicular to a plate *Appl. Math. Comput.* **200** 459–64
[8] Fetecau C, Jamil M, Fetecau C and Siddique I 2009 A note on the second problem of Stokes for Maxwell fluids *Int. J. Non-Linear Mech.* **44** 1085–90
[9] Adegbie K S, Omowaye A J, Disu A B and Animasaun I L 2015 Heat and mass transfer of upper convected Maxwell fluid flow with variable thermo-physical properties over a horizontal melting surface *Appl. Math.* **6** 1362–79
[10] Nadeem S, Mehmood R and Akbar N S 2013 Non-orthogonal stagnation point flow of a nano non-Newtonian fluid towards a stretching surface with heat transfer *Int. J. Heat Mass Transfer* **57** 679–89
[11] Majeed A, Zeeshan A and Ellahi R 2017 Chemical reaction and heat transfer on boundary layer Maxwell Ferro-fluid flow under magnetic dipole with Soret and suction effects *Eng. Sci. Tech. Int. J.* **20** 1122–8
[12] Hayat T, Ahmad S, Khan M I and Alsaedi A 2018 Simulation of ferromagnetic nanomaterial flow of Maxwell fluid *Res. Phys.* **8** 34–40
[13] Ramzan M, Bilal M, Chung J D and Farooq U 2016 Mixed convective flow of Maxwell nanofluid past a porous vertical stretched surface—an optimal solution *Res. Phys.* **6** 1072–9
[14] Abdelsalam S I and Bhatti M M 2019 New insight into AuNP applications in tumor treatment and cosmetics through wavy annuli at the nanoscale *Sci. Rep.* **9** 1–14
[15] Abdelsalam S I and Bhatti M M 2018 The study of non-Newtonian nanofluid with Hall and ion slip effects on peristaltically induced motion in a non-uniform channel *RSC Adv.* **8** 7904–15
[16] Abdelsalam S I and Bhatti M M 2018 The impact of impinging TiO_2 nanoparticles in Prandtl nanofluid along with endoscopic and variable magnetic field effects on peristaltic blood flow, multidiscipline modeling in *Mater. Struct.* **14** 530–48
[17] Abd Elmaboud Y, Abdelsalam S I, Mekheimer K S and Vafai K 2019 Electromagnetic flow for two-layer immiscible fluids *Engi. Sci. Tech., Int. J.* **22** 237–48
[18] Abdelsalam S I and Vafai K 2017 Combined effects of magnetic field and rheological properties on the peristaltic flow of a compressible fluid in a microfluidic channel *Eur. J. Mech.* B **65** 398–411
[19] Abdelsalam S I and Vafai K 2017 Particulate suspension effect on peristaltically induced unsteady pulsatile flow in a narrow artery: blood flow model *Math. Biosci.* **283** 91–105
[20] Merkin J H 1995 A model for isothermal homogeneous–heterogeneous reactions in boundary layer flow *Math. Comput. Modell.* **24** 125–36
[21] Chaudhary M A and Merkin J H 1995 A simple isothermal model for homogeneous–heterogeneous reactions in boundary layer flow. II Different diffusivities for reactant and autocatalyst *Fluid Dyn. Res.* **16** 335–9

[22] Bachok N, Ishak A and Pop I 2011 On the stagnation-point flow towards a stretching sheet with homogeneous–heterogeneous reactions effects *Commun. Nonlinear Sci. Numer. Simul.* **16** 4296–302
[23] Kameswaran P K, Shaw S, Sibanda P and Murthy P V S N 2013 Homogeneous–heterogeneous reactions in a nano fluid flow due to porous stretching sheet *Int. J. Heat Mass Transfer* **57** 465–72
[24] Imtiaz M, Hayat T, Alsaedi A and Hobiny A 2016 Homogeneous–heterogeneous reactions in MHD flow due to an unsteady curved stretching surface *J. Mol. Liq.* **221** 245–53
[25] Hayat T, Hussain Z, Muhammad T and Alsaedi A 2016 Effects of homogeneous and heterogeneous reactions in flow of nanofluids over a nonlinear stretching surface with variable surface thickness *J. Mol. Liq.* **221** 1121–7
[26] Abbas Z and Sheikh M 2017 Numerical study of homogeneous–heterogeneous reactions on stagnation point flow of ferro fluid with non-linear slip condition *Chin. J. Chem. Eng.* **25** 11–7
[27] Khan M I, Waqas M, Hayat T and Alsaedi A 2017 A comparative study of Casson fluid with homogeneous–heterogeneous reactions *J. Colloid Interface Sci.* **498** 85–90
[28] Kuznetsov A V 2005 Thermo-Bioconvection in a suspension of oxytactic bacteria *Int. Commun. Heat Mass Transfer* **32** 991–9
[29] Geng P and Kuznetsov A V 2004 Effect of small solid particles on the development of bioconvection plumes *Int. Commun. Heat Mass Transfer* **31** 629–38
[30] Geng P and Kuznetsov A V 2005 Settling of bidispersed small solid particles in a dilute suspension containing gyrotactic micro-organisms *Int. J. Eng. Sci.* **43** 992–1010
[31] Geng P and Kuznetsov A V 2005 Introducing the concept of effective diffusivity to evaluate the effect of bioconvection on small solid particles *Int. J. Transp. Phenom.* **7** 321–38
[32] Zuhra S, Khan N S, Shah Z, Islam S and Bonyah E 2018 Simulation of bioconvection in the suspension of second grade nanofluid containing nanoparticles and gyrotactic microorganisms *AIP Adv.* **8** 105210
[33] Ur Rehman K, Malik A A, Tahir M and Malik M Y 2018 Undersized description on motile gyrotactic micro-organisms individualities in MHD stratified water-based Newtonian nanofluid *Res. Phys.* **8** 981–7
[34] Avramenko A A and Kuznetsov A V 2004 Stability of a suspension of gyrotactic microorganisms in superimposed fluid and porous layers *Int. Commun. Heat Mass Transfer* **31** 1057–66
[35] Alloui Z, Nguyen T H and Bilgen E 2007 Numerical investigation of thermo bioconvection in a suspension of gyrotactic microorganisms *Int. J. Heat Mass Transfer* **50** 1435–41
[36] Bejan A 1979 A study of entropy generation in fundamental convective heat transfer *J. Heat Transfer* **101** 718–25
[37] Akmal N, Sagheer M and Hussain S 2018 Numerical study focusing on the entropy analysis of MHD squeezing flow of a nanofluid model using Cattaneo–Christov theory *AIP Adv.* **8** 055201
[38] Dalir N 2014 Numerical study of entropy generation for forced convection flow and heat transfer of a Jeffrey fluid over a stretching sheet *Alexandria Eng. J.* **53** 769–78
[39] Shojaeian M and Kosar A 2014 Convective heat transfer and entropy generation analysis on Newtonian and non-Newtonian fluid flows between parallel-plates under slip boundary conditions *Int. J. Heat Mass Transfer* **70** 664–73
[40] Kefayati G H R 2018 Double-diffusive natural convection and entropy generation of Bingham fluid in an inclined cavity *Int. J. Heat Mass Transfer* **116** 762–812
[41] Qiu S, Xie Z, Chen L, Yang A and Zhou J 2018 Entropy generation analysis for convective heat transfer of nanofluids in tree-shaped network flowing channels *Therm. Sci. Eng. Prog.* **5** 546–54
[42] Hayat T, Khan M I, Qayyum S and Alsaedi A 2018 Entropy generation in flow with silver and copper nanoparticles *Colloids Surf.* A **539** 335–46
[43] Afridi M I and Qasim M 2018 Entropy generation and heat transfer in boundary layer flow over a thin needle moving in a parallel stream in the presence of nonlinear Rosseland radiation *Int. J. Therm. Sci.* **123** 117–28
[44] Khan N B, Ibrahim Z, Khan M I, Hayat T and Javed M F 2018 VIV study of an elastically mounted cylinder having low mass-damping ratio using RANS model *Int. J. Heat Mass Transfer* **121** 309–14
[45] Han S, Zheng L, Li C and Zhang X 2014 Coupled flow and heat transfer in viscoelastic fluid with Cattaneo–Christov heat flux model *Appl. Math. Lett.* **38** 87–93
[46] Turkyilmazoglu M 2016 An effective approach for evaluation of the optimal convergence control parameter in the homotopy analysis method *Filomat* **30** 1633–50
[47] Liao S J 2010 An optimal homotopy analysis approach for strongly nonlinear differential equations *Commun. Nonlinear Sci. Numer. Simul.* **15** 2003–16
[48] Mushtaq A, Mustafa M, Hayat T and Alsaedi A 2014 On the numerical solution of the nonlinear radiation heat transfer problem in a three-dimensional flow *Z. Naturforsch.* A **69** 705–13
[49] Wang C Y 1984 The three-dimensional flow due to a stretching at surface *Phys. Fluids* **27** 1915–7
[50] Liu I and Andersson H I 2008 Heat transfer over a bidirectional stretching sheet with variable thermal conditions *Int. J. Heat Mass Transfer* **51** 4018–24